Predictions of synthesizing elements with $Z = 119$ and 120 in fusion reactions

Ming-Hao Zhang [1,2], Yu-Hai Zhang,[1,2] Ying Zou,[1,2] Chen Wang,[1,2] Long Zhu,[3] and Feng-Shou Zhang [1,2,4,*]

[1]*The Key Laboratory of Beam Technology of Ministry of Education, College of Nuclear Science and Technology,*
Beijing Normal University, Beijing 100875, China

[2]*Institute of Radiation Technology, Beijing Academy of Science and Technology, Beijing 100875, China*

[3]*Sino-French Institute of Nuclear Engineering and Technology, Sun Yat-sen University, Zhuhai 519082, China*

[4]*Center of Theoretical Nuclear Physics, National Laboratory of Heavy Ion Accelerator of Lanzhou, Lanzhou 730000, China*

Within the framework of the dinuclear system model, the experimentally accessible projectile-target combinations are predicted for the production of new superheavy elements with $Z = 119$ and $Z = 120$. The entrance channel effect and the isotopic dependence of targets and projectiles on the capture, fusion, and survival stages of the fusion reaction are discussed. The reactions ^{45}Sc $+$ ^{249}Cf and ^{50}V $+$ ^{246}Cm are found to be promising candidates for the synthesis of the element with $Z = 119$, achieving the maximal evaporation residue cross sections of 0.288 pb at an incident energy of 211.2 MeV and 0.237 pb at an incident energy of 226.2 MeV, respectively. Meanwhile, the element with $Z = 120$ can be synthesized through the reaction ^{46}Ti $+$ ^{249}Cf with a maximal evaporation residue cross section of 0.040 pb at 221.8 MeV.

I. INTRODUCTION

One of the forefront issues in nuclear physics is exploring the eighth period of the periodic table and achieving the location of next shell closure beyond $Z = 82$ and $N = 126$. The macroscopic-microscopic method, the Skyrme-Hartree-Fock theory, and the relativistic mean-field theory predict the proton shell at $Z = 114, 120, 124$, or 126 and the neutron shell at $N = 172$ or 184 [1–4], and the island of stability is expected to be near this region [5]. By synthesizing new superheavy elements (SHEs), the location of the island of stability can be precisely determined, and the shell structure of superheavy nuclei can be further investigated. Through cold fusion reactions based on ^{208}Pb or ^{209}Bi targets, the SHEs with $Z = 107$–113 were synthesized at GSI and RIKEN [6,7]. However, It was observed that the evaporation residue (ER) cross section decreases exponentially with the increase of the charge number of the compound nucleus [8]. In response to this challenge, researchers in Dubna shifted their focus to hot fusion reactions utilizing a ^{48}Ca beam and actinide targets, leading to the successful synthesis of SHEs with $Z = 114$–118 [9–13]. This achievement marks the completion of the seventh period of the periodic table.

To date, modern accelerators such as RILAC of RIKEN [14], DC-280 and U-400 of the SHE Factory in Dubna [15,16], SFC of HIRFL, and UNILAC of GSI [17,18] have achieved significant progress in the synthesis of new isotopes with $Z \leqslant 118$ [6,8,19–24]. Moreover, several attempts also have been made to synthesize the SHEs with $Z = 119$ and 120. Initially, Dubna attempted to synthesize the SHE with $Z = 120$ using the reaction ^{58}Fe $+$ ^{244}Pu in 2009 [25], yet

no corresponding α decay chain was observed. In 2016, GSI attempted to synthesize the element with $Z = 120$ through the reaction ^{54}Cr $+$ ^{248}Cm [26] and observed three α decay chains related to ^{299}120. Unfortunately, these were later identified as random events [27]. Additionally, GSI searched for the new elements $Z = 119$ and 120 via reactions ^{50}Ti $+$ ^{249}Bk and ^{50}Ti $+$ ^{249}Cf in 2020 [28], but no evidence confirming the discovery of new SHEs was detected. In 2022, RIKEN extracted the quasielastic barrier distribution of reaction ^{51}V $+$ ^{248}Cm and deduced the optimal reaction energy to synthesize element 119 for this reaction [29]. The synthesis of new superheavy nuclei has encountered various challenges, including the short half-lives and high instability of both the target materials and the synthesized nuclei [30,31]. Moreover, the ER cross section, which is typically in the order of picobarns [32], has reached the limitation of experimental detection. Hence, it is essential to construct accurate theoretical predictions of the proper reaction systems and incident energies for future experiments.

Based on ample experimental data, many theoretical approaches describing fusion-evaporation reactions have been developed, such as the improved quantum molecular dynamics (ImQMD) model [33,34], the fusion-by-diffusion (FBD) model [35–37], the cluster dynamical decay model [38], the time-dependent Hartree-Fock (TDHF) theory [37,39–41], the two-step model [42–44], and multidimensional Langevin-type dynamical equations [45–47]. The dinuclear system (DNS) model was also proved to be reliable in describing the production of new SHEs [48–59]. Within the DNS model, the fusion dynamics is viewed as a diffusion process occurring along proton and neutron degrees of freedom. The process of nucleon transfer is coupled to the relative motion by solving a group of master equations, governed by the potential energy surface with consideration of nuclear structure effects [53].

---

*Corresponding author: fszhang@bnu.edu.cn

In this paper, the reliability of the DNS model has been tested by comparing the theoretical results with experimental data. Considering the feasibility of experimentation, we choose actinide targets that have been practically used in experiments with corresponding stable projectiles to predict the synthesis of new SHEs with $Z = 119$ and 120.

This article is organized as follows: In Sec. II, we introduce the theoretical details of the DNS model and verify the reliability of this model. In Sec. III, the maximal ER cross sections and optimal incident energies corresponding to the synthesis of the new isotopes are predicted. The isotopic dependence of targets and the entrance channel effect for synthesizing the SHE with $Z = 119$ and the isotopic dependence of projectiles are systematically discussed. Finally in Sec. IV we present a summary of this work.

II. THE MODEL

In the DNS model, the fusion-evaporation process can be elucidated through a three-step process, including capture, fusion, and survival stages. Initially, the formation of a dinuclear system occurs when the colliding nuclei overcome the Coulomb barrier height V_B. Subsequently, the dinuclear system undergoes nucleon transfer and forms a compound nucleus. Finally, to attain the ground state, the excited compound nucleus deexcites via fission or evaporating particles. Therefore, the ER cross section can be calculated over the partial waves J as follows:

$$\sigma_{ER}(E_{c.m.}) = \frac{\pi \hbar^2}{2\mu E_{c.m.}} \sum_J (2J+1) T(E_{c.m.}, J)$$
$$\times P_{CN}(E_{c.m.}, J) W_{sur}(E_{c.m.}, J), \quad (1)$$

where $E_{c.m.}$ denotes the center-of-mass energy. $T(E_{c.m.}, J)$ is the transmission probability for overcoming the Coulomb potential barrier to form a DNS. $P_{CN}(E_{c.m.}, J)$ represents the complete fusion probability [60], and $W_{sur}(E_{c.m.}, J)$ represents the survival probability of the compound nucleus [61].

A. Transmission probability and capture cross section

For the fusion reactions, the transmission probability $T(E_{c.m.}, B, J)$ can be calculated by the Ahmed formula with the reduced mass μ [62,63]:

$$T(E_{c.m.}, B, J) = \frac{1 - \exp(-4\pi\alpha)}{1 + \exp[2\pi(\beta_J - \alpha)]}, \quad (2)$$

where

$$\alpha = \frac{\sqrt{2\mu E_{c.m.}}}{\hbar} \alpha_M$$

and

$$\beta_J = \frac{\sqrt{2\mu \left(B + \frac{\hbar^2}{2\mu R_B^2(J)} J(J+1)\right)}}{\hbar} \alpha_M,$$

and α_M is the Morse parameter [64]. The nucleus-nucleus interaction potential with quadrupole deformation can be written as [53]

$$V(R, \beta_1, \beta_2, \theta_1, \theta_2) = \frac{1}{2} C_1 (\beta_1 - \beta_1^0)^2 + \frac{1}{2} C_2 (\beta_2 - \beta_2^0)^2$$
$$+ V_C(R, \beta_1, \beta_2, \theta_1, \theta_2)$$
$$+ V_N(R, \beta_1, \beta_2, \theta_1, \theta_2). \quad (3)$$

Here β_1 (β_2) and β_1^0 (β_2^0) are the parameters of dynamical quadrupole deformation and static deformation for the projectile (target). θ_1 (θ_2) is the angle between the collision direction and the symmetry axes of the statically deformed projectile (target). $C_{1,2}$ are the stiffness parameters of the nuclear surface, which are calculated with the liquid drop model [65]:

$$C_i = (\lambda - 1) \left[(\lambda + 2) R_{0,i}^2 \sigma - \frac{3}{2\pi} \frac{Z_i^2 e^2}{R_{0,i}(2\lambda + 1)} \right], \quad (4)$$

where λ is the level of the dynamical deformation. Here we only consider the quadrupole deformation ($\lambda = 2$). The Coulomb potential V_C can be calculated from the Wang formula [66]:

$$V_C(R, \beta_1, \beta_2, \theta_1, \theta_2) = \frac{Z_1 Z_2 e^2}{R} + \sqrt{\frac{9}{20\pi}} \frac{Z_1 Z_2 e^2}{R^3} \sum_{i=1,2} R_i^2 \beta_2^{(i)} P_2(\cos\theta_i) + \frac{3}{7\pi} \frac{Z_1 Z_2 e^2}{R^3} \sum_{i=1,2} R_i^2 \left[\beta_2^{(i)} P_2(\cos\theta_i) \right]^2. \quad (5)$$

The nuclear potential V_N can be written as [67]:

$$V_N(R, \beta_1, \beta_2, \theta_1, \theta_2) = -V_0 \left\{ 1 + \exp \left[\frac{r - \sum_{i=1,2} R_i \left(1 + \sqrt{5/4\pi} \beta_2^{(i)} P_2(\cos\theta_i) \right)}{a} \right] \right\}^{-1}. \quad (6)$$

Considering the barrier distribution, the transmission probability can be expressed as

$$T(E_{c.m.}, J) = \int f(B) T(E_{c.m.}, B, J) dB. \quad (7)$$

Here

$$f(B) = \frac{1}{N} \exp \left[-\left(\frac{B - B_m}{\Delta_{1,2}} \right)^2 \right]$$

is the barrier distribution function with an asymmetric Gaussian form. The barrier distribution parameters B_m, Δ_1 and Δ_2 are given by the fitting for the spherical and deformed systems [68] and N is the normalization coefficient. The capture cross section σ_{cap} can be represented by the following formula [69]:

$$\sigma_{cap}(E_{c.m.}) = \frac{\pi \hbar^2}{2\mu E_{c.m.}} \sum_J (2J+1) T(E_{c.m.}, J). \quad (8)$$

B. Fusion process and the fusion probability

The complete fusion probability $P_{CN}(E_{c.m.}, J)$ can be evaluated by considering the fusion process as a diffusion of dinuclear system in the mass asymmetry degree $\eta = (A_P - A_T)/(A_P + A_T)$. For a fragment (Z_1, N_1) with the excitation energy E_1 at the instantaneous time t, the distribution function $P(Z_1, N_1, E_1, t)$ can be obtained by the following master equation:

$$
\begin{aligned}
\frac{dP(Z_1, N_1, E_1, t)}{dt} \\
= \sum_{Z_1'} W_{Z_1,N_1;Z_1',N_1}(t) \\
\times [d_{Z_1,N_1} P(Z_1', N_1, E_1, t) - d_{Z_1',N_1} P(Z_1, N_1, E_1, t)] \\
+ \sum_{N_1'} W_{Z_1,N_1;Z_1,N_1'}(t) \\
\times [d_{Z_1,N_1} P(Z_1, N_1', E_1, t) - d_{Z_1,N_1'} P(Z_1, N_1, E_1, t)] \\
- [\Lambda_{qf}(\Theta(t)) + \Lambda_{fis}(\Theta(t))] P(Z_1, N_1, E_1, t).
\end{aligned}
\tag{9}
$$

In this formula, $W_{Z_1,N_1;Z_1',N_1}$ represents the mean transition probability from (Z_1, N_1) to (Z_1', N_1) [70], d_{Z_1,N_1} indicates the microscopic dimension for the corresponding macroscopic variables. Λ_{qf} and Λ_{fis} denote the quasi-fission and fission probabilities [71,72], respectively.

In the fusion stage, the nucleon transfer process is driven by the potential energy surface defined as [73]

$$
\begin{aligned}
U(Z_1, N_1, Z_2, N_2, R, \beta_1, \beta_2) \\
= E_B(Z_1, N_1) + E_B(Z_2, N_2) - E_B(Z, N) \\
+ V_{CN}(Z_1, N_1, Z_2, N_2, R, \beta_1, \beta_2).
\end{aligned}
\tag{10}
$$

Here, $E_B(Z, N)$, $E_B(Z_{1(2)}, N_{1(2)})$ are the binding energies of the compound nucleus and the projectile (target) given by the macroscopic-microscopic model [2]. V_{CN} represents the nucleus-nucleus interaction potential, which comprises the Coulomb potential and the nuclear potential, defined as follows:

$$
\begin{aligned}
V_{CN}(Z_1, N_1, Z_2, N_2, R, \beta_1, \beta_2) \\
= V_C(Z_1, N_1, Z_2, N_2, R, \beta_1, \beta_2) \\
+ V_N(Z_1, N_1, Z_2, N_2, R, \beta_1, \beta_2).
\end{aligned}
\tag{11}
$$

In the fusion process, the nucleon transfer process occurs at the bottom of the potential pocket. This minimal trajectory of the potential energy surface along the degree of η is defined as the driving potential. The fusion probability can be obtained by summing the distribution probabilities of the fragments that cross the Businaro-Gallone (B.G.) point (the highest point of the driving potential). The gap in the driving potential between the B.G. point and the incident point is defined as the inner fusion barrier $B_{fus} = U(\eta_{B.G.}) - U(\eta_i)$. If the system manages to overcome the inner fusion barrier, the compound nucleus is formed; otherwise, the quasifission process occurs. Thus the fusion probability can be expressed as follows [74]:

$$
P_{CN}(E_{c.m.}, J) = \int f(B) P_{CN}(E_{c.m.}, J, B) dB.
\tag{12}
$$

Here, $P_{CN}(E_{c.m.}, J, B)$ is the formation probability of the compound nucleus, which is given by

$$
\begin{aligned}
P_{CN}(E_{c.m.}, J, B) \\
= \sum_{Z_1=1}^{Z_{B.G.}} \sum_{N_1=1}^{N_{B.G.}} P[Z_1, N_1, E_1, \tau_{int}(E_{c.m.}, J, B)],
\end{aligned}
\tag{13}
$$

with the interaction time $\tau_{int}(E_{c.m.}, J, B)$ obtained through the deflection function method [75].

C. The survival probability of excited compound nucleus

In the survival stage, the excited compound nucleus can deexcite through particles and γ-ray emission or through fission. With the negligible impact of γ-ray and charged-particle emission, the primary competition lies between fission and neutron evaporation [52]. When x neutrons are evaporated, the survival probability can be calculated by the statistical model as

$$
W_{sur}(E_{CN}^*, x, J) = P(E_{CN}^*, x, J) \prod_{i=1}^{x} \left[\frac{\Gamma_n(E_i^*, J)}{\Gamma_n(E_i^*, J) + \Gamma_f(E_i^*, J)} \right].
\tag{14}
$$

$P(E_{CN}^*, x, J)$ represents the realization probability [76] when the compound nucleus evaporates x neutrons with the excitation energy E_{CN}^*. E_i^* is the excitation energy before evaporating the ith neutron, which can be given by $E_{i+1}^* = E_i^* - B_i^n - 2T_i$, with the initial excitation energy $E_1^* = E_{CN}^*$. B_i^n is the separation energy of the ith neutron [2] and $T_i = \sqrt{E_i/a}$ is the nuclear temperature before evaporating the ith neutron. The level density parameter a can be taken as $a = A/12$ MeV or the expression dependent on the shell correction and the E_{CN}^* values [58].

The partial decay widths for the evaporation of neutron can be estimated by the Weisskopf-Ewing theory [77]:

$$
\begin{aligned}
\Gamma_n(E^*, J) = \frac{(2s_n + 1)m_n}{\pi^2 \hbar^2 \rho(E^*, J)} \\
\times \int_{I_n} \varepsilon \rho(E^* - B_n - \varepsilon, J) \sigma_{inv}(\varepsilon) d\varepsilon,
\end{aligned}
\tag{15}
$$

where $I_n = [0, E^* - B_n - \delta - \frac{1}{a}]$. $\delta = 0$, Δ, or 2Δ for the odd-odd, odd-even and even-even nuclei; $\Delta = 12/\sqrt{A}$ MeV. B_n denotes the neutron separation energy. The level density ρ is calculated with the Fermi-gas model [78] and σ_{inv} represents the inverse reaction cross section for the particle ν with the channel energy ε [79].

The fission decay width Γ_f can be calculated with the Bohr-Wheeler transition-state method [52]:

$$
\begin{aligned}
\Gamma_f(E^*, J) = \frac{1}{2\pi \rho_f(E^*, J)} \\
\times \int_{I_f} \frac{\rho_f(E^* - B_f - \varepsilon, J) d\varepsilon}{1 + \exp[-2\pi(E^* - B_f - \varepsilon)/\hbar\omega]},
\end{aligned}
\tag{16}
$$

with $I_f = [0, E^* - B_f - \delta - \frac{1}{a_f}]$. Here $a_f/a = 1.1$ is related to the rate of nuclear structure evaluation from the ground state to the saddle point [80,81].
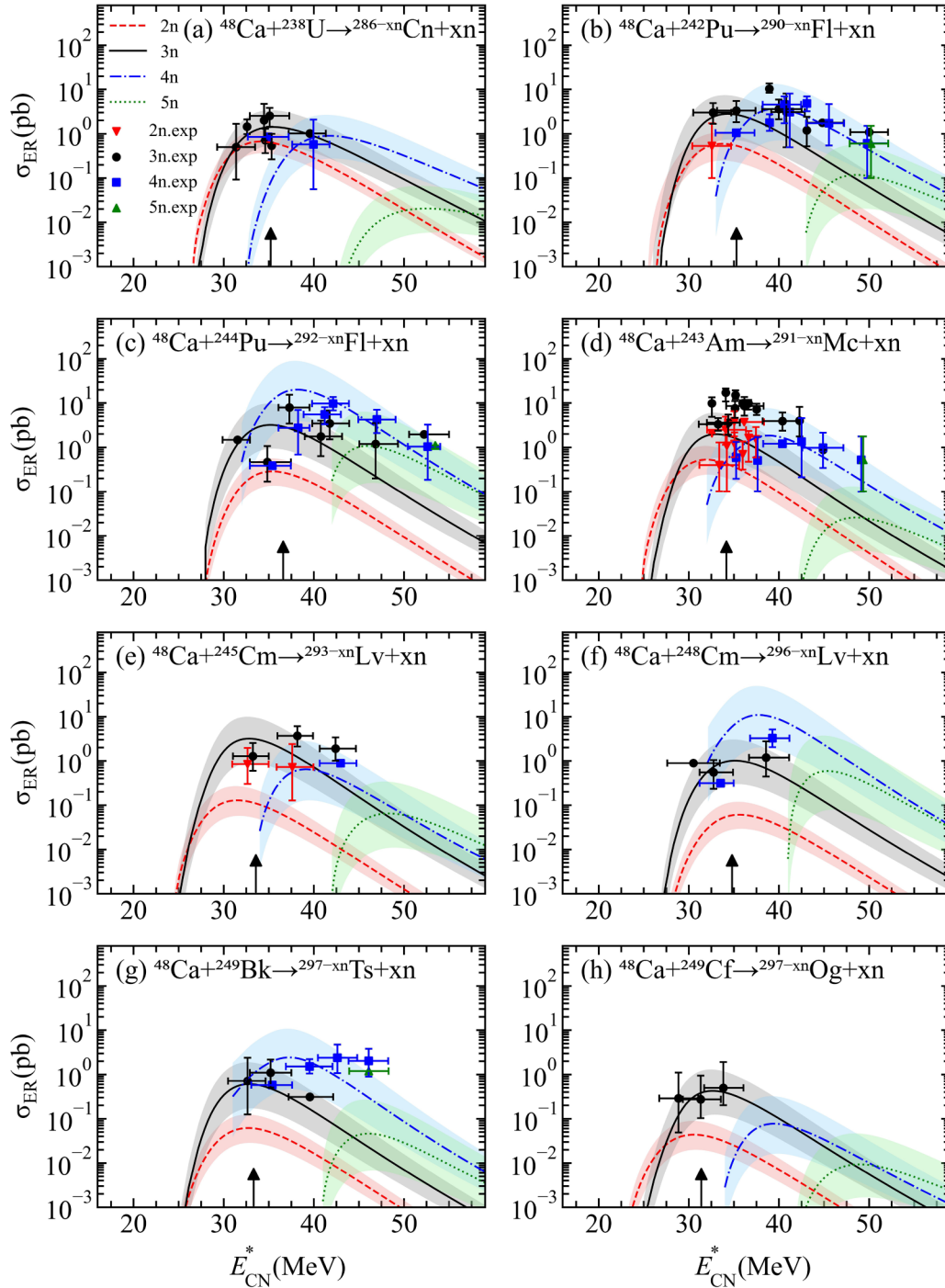
FIG. 1. Comparison of the calculated results with the available experimental data [9,11,23,86–96]. The calculated ER cross sections in the 2n, 3n, 4n, and 5n channels are denoted by the red dashed lines, black solid lines, blue dash-dot lines, and green dotted lines, respectively. The black arrows denote the positions of the Coulomb barrier heights in side-side collisions $V_{\mathrm{B}}^{\mathrm{side}}$ [29,97]. The experimental data for the 2n-, 3n-, 4n-, and 5n-emission channels are presented by the solid red inverted triangles, black circles, blue squares, and green triangles with the error bars, respectively.

Considering the temperature dependence [82,83], the fission barrier of the rotating nucleus can be written as follows:

$$B_{\mathrm{f}}(E^*, J) = B_{\mathrm{f}}^{\mathrm{LD}}\left(1 - x_{\mathrm{LD}}T_i^2\right)$$
$$+ B_{\mathrm{f}}^{\mathrm{M}}(E^* = 0, J)\exp\left(-\frac{E^*}{E_{\mathrm{D}}}\right)$$

$$- \left(\frac{\hbar^2}{2J_{\mathrm{g.s.}}} - \frac{\hbar^2}{2J_{\mathrm{s.d.}}}\right)J(J+1), \qquad (17)$$

where the macroscopic part $B_{\mathrm{f}}^{\mathrm{LD}}$ and the microscopic part $B_{\mathrm{f}}^{\mathrm{M}}$ are determined by the liquid-drop model and the microscopic shell correction [2]. The temperature dependent parameter

TABLE I. Some feasible reaction systems for producing isotopes with $Z = 119$ via the DNS model and other theoretical models. The half-lives of corresponding targets are taken from Ref. [100].

Isotope	Reaction	$T_{1/2}^{\text{target}}$	$E_{\text{c.m.}}$ (MeV)	E_{CN}^* (MeV)	σ_{ER} (pb)	Reference
$^{290}119$	^{243}Am(^{50}Cr, $3n$)	7.36×10^3 yr	231.7	35.0	$0.017^{+0.028}_{-0.011}$	This work
$^{291}119$	^{249}Cf(^{45}Sc, $3n$)	351.00 yr	211.2	35.0	$0.288^{+0.493}_{-0.190}$	This work
	^{244}Cm(^{50}V, $3n$)	18.10 yr	229.6	34.0	$0.087^{+0.149}_{-0.058}$	This work
	^{249}Bk(^{46}Ti, $4n$)	330.00 d	223.4	44.0	$0.016^{+0.039}_{-0.012}$	This work
$^{292}119$	^{249}Bk(^{46}Ti, $3n$)	330.00 d	213.4	34.0	$0.143^{+0.255}_{-0.096}$	This work
	^{245}Cm(^{50}V, $3n$)	8.42×10^3 yr	227.4	34.0	$0.046^{+0.082}_{-0.031}$	This work
	^{244}Cm(^{51}V, $3n$)	18.10 yr	232.9	34.0	$0.024^{+0.043}_{-0.016}$	This work
	^{243}Am(^{52}Cr, $3n$)	7.36×10^3 yr	237.4	34.0	$0.021^{+0.038}_{-0.014}$	This work
$^{293}119$	^{246}Cm(^{50}V, $3n$)	4.71×10^3 yr	226.2	33.0	$0.237^{+0.437}_{-0.162}$	This work
	^{245}Cm(^{51}V, $3n$)	8.42×10^3 yr	230.8	33.0	$0.136^{+0.247}_{-0.092}$	This work
	^{243}Am(^{53}Cr, $3n$)	7.36×10^3 yr	237.7	33.0	$0.097^{+0.178}_{-0.066}$	This work
	^{249}Bk(^{48}Ti, $4n$)	330.00 d	227.7	42.0	$0.014^{+0.037}_{-0.010}$	This work
	^{243}Am(^{54}Cr, $4n$)	7.36×10^3 yr	248.9	42.0	$0.002^{+0.005}_{-0.001}$	This work
$^{294}119$	^{249}Bk(^{48}Ti, $3n$)	330.00 d	219.7	34.0	$0.029^{+0.054}_{-0.020}$	This work
	^{246}Cm(^{51}V, $3n$)	4.71×10^3 yr	230.7	34.0	$0.023^{+0.043}_{-0.016}$	This work
	^{248}Cm(^{50}V, $4n$)	3.48×10^5 yr	231.0	40.0	$0.010^{+0.027}_{-0.007}$	This work
	^{243}Am(^{54}Cr, $3n$)	7.36×10^3 yr	243.4		0.002	[101]
	^{243}Am(^{54}Cr, $3n$)	7.36×10^3 yr	239.9	33.0	$0.007^{+0.012}_{-0.005}$	This work
$^{295}119$	^{248}Cm(^{50}V, $3n$)	3.48×10^5 yr	223.0	32.0	$0.173^{+0.326}_{-0.119}$	This work
	^{249}Bk(^{49}Ti, $3n$)	330.00 d	220.9	33.0	$0.091^{+0.168}_{-0.062}$	This work
	^{249}Bk(^{50}Ti, $4n$)	330.00 d	236.2	43.7	0.057	[102]
	^{249}Bk(^{50}Ti, $4n$)	330.00 d	232.8		0.036	[36]
	^{249}Bk(^{50}Ti, $4n$)	330.00 d	243.6		0.006	[101]
	^{249}Bk(^{50}Ti, $4n$)	330.00 d	234.2		0.035	[103]
	^{249}Bk(^{50}Ti, $4n$)	330.00 d	236.0		0.064	[104]
	^{249}Bk(^{50}Ti, $4n$)	330.00 d	232.6		0.036	[105]
	^{249}Bk(^{50}Ti, $4n$)	330.00 d	231.8	40.0	$0.010^{+0.029}_{-0.008}$	This work
	^{248}Cm(^{51}V, $4n$)	3.48×10^5 yr	248.6		0.001	[101]
	^{248}Cm(^{51}V, $4n$)	3.48×10^5 yr	236.1		0.006	[105]
	^{248}Cm(^{51}V, $4n$)	3.48×10^5 yr	237.0		0.010	[104]
	^{248}Cm(^{51}V, $4n$)	3.48×10^5 yr	235.0	40.0	$0.013^{+0.035}_{-0.010}$	This work
$^{296}119$	^{244}Pu(^{55}Mn, $3n$)	8.00×10^7 yr	240.1	32.0	$0.010^{+0.018}_{-0.007}$	This work
	^{249}Bk(^{50}Ti, $3n$)	330.00 d	233.6	41.1	0.039	[102]
	^{249}Bk(^{50}Ti, $3n$)	330.00 d	225.2		0.030	[36]
	^{249}Bk(^{50}Ti, $3n$)	330.00 d	226.0		0.048	[101]
	^{249}Bk(^{50}Ti, $3n$)	330.00 d	223.1		0.035	[103]
	^{249}Bk(^{50}Ti, $3n$)	330.00 d	225.0		0.031	[105]
	^{249}Bk(^{50}Ti, $3n$)	330.00 d	224.0		0.012	[104]
	^{249}Bk(^{50}Ti, $3n$)	330.00 d	225.8	34.0	$0.008^{+0.015}_{-0.006}$	This work
	^{248}Cm(^{51}V, $3n$)	3.48×10^5 yr	230.1		0.001	[101]
	^{248}Cm(^{51}V, $3n$)	3.48×10^5 yr	228.3		0.003	[105]
	^{248}Cm(^{51}V, $3n$)	3.48×10^5 yr	227.0		0.005	[104]
	^{248}Cm(^{51}V, $3n$)	3.48×10^5 yr	229.0	34.0	$0.013^{+0.024}_{-0.009}$	This work

$x_{\text{LD}} = 0.04$ [82]. $E_{\text{D}} = 25$ MeV [56] is the shell damping energy which is responsible for the diminishing shell effects as the excitation energy of the compound nucleus increases. $J_{\text{g.s.}}$ and $J_{\text{s.d.}}$ are the moments of inertia of the compound nucleus in the ground state and at the saddle point, respectively [84,85].

D. Verification of the DNS model

In order to verify the reliability of utilizing the DNS model for predicting the ER cross sections of synthesizing the new superheavy nuclei, the theoretical results based on the DNS model are compared with the corresponding experimental data for the fusion reactions ^{48}Ca + ^{238}U $\rightarrow$ $^{286-xn}$Cn + xn,

TABLE II. The same as in Table I, but for producing isotopes with $Z = 120$.

Isotope	Reaction	$T_{1/2}^{\text{target}}$	$E_{\text{c.m.}}$ (MeV)	E_{CN}^* (MeV)	σ_{ER} (pb)	References
$^{292}120$	$^{249}\text{Cf}(^{46}\text{Ti}, 3n)$	351.00 yr	221.8	36.0	$0.040^{+0.060}_{-0.025}$	This work
	$^{245}\text{Cm}(^{50}\text{Cr}, 3n)$	8.42×10^3 yr	236.6	36.0	$0.011^{+0.016}_{-0.007}$	This work
$^{293}120$	$^{249}\text{Cf}(^{47}\text{Ti}, 3n)$	351.00 yr	222.5	36.0	$0.014^{+0.023}_{-0.009}$	This work
$^{294}120$	$^{249}\text{Cf}(^{48}\text{Ti}, 3n)$	351.00 yr	227.6	36.0	$0.010^{+0.016}_{-0.007}$	This work
$^{295}120$	$^{249}\text{Cf}(^{50}\text{Ti}, 4n)$	351.00 yr	241.5	43.4	0.045	[102]
	$^{249}\text{Cf}(^{50}\text{Ti}, 4n)$	351.00 yr	239.3		0.006	[36]
	$^{249}\text{Cf}(^{50}\text{Ti}, 4n)$	351.00 yr	241.3		0.003	[103]
	$^{249}\text{Cf}(^{50}\text{Ti}, 4n)$	351.00 yr	252.1		0.0007	[101]
	$^{249}\text{Cf}(^{50}\text{Ti}, 4n)$	351.00 yr	240.0		0.029	[104]
	$^{249}\text{Cf}(^{50}\text{Ti}, 4n)$	351.00 yr	240.7		$0.0003^{+0.0007}_{-0.0002}$	This work
$^{296}120$	$^{249}\text{Cf}(^{50}\text{Ti}, 3n)$	351.00 yr	236.6	38.5	0.042	[102]
	$^{249}\text{Cf}(^{50}\text{Ti}, 3n)$	351.00 yr	229.1		0.006	[36]
	$^{249}\text{Cf}(^{50}\text{Ti}, 3n)$	351.00 yr	234.1		0.008	[101]
	$^{249}\text{Cf}(^{50}\text{Ti}, 3n)$	351.00 yr	227.4		0.020	[103]
	$^{249}\text{Cf}(^{50}\text{Ti}, 3n)$	351.00 yr	232.8		0.023	[106]
	$^{249}\text{Cf}(^{50}\text{Ti}, 3n)$	351.00 yr	228.9		0.020	[104]
	$^{249}\text{Cf}(^{50}\text{Ti}, 3n)$	351.00 yr	231.7		$0.0023^{+0.0037}_{-0.0015}$	This work
	$^{249}\text{Bk}(^{51}\text{V}, 4n)$	330.00 d	253.3		0.0002	[101]
	$^{249}\text{Bk}(^{51}\text{V}, 4n)$	330.00 d	242.0		0.0018	[104]
	$^{249}\text{Bk}(^{51}\text{V}, 4n)$	330.00 d	241.0		$0.0009^{+0.002}_{-0.0006}$	This work
$^{297}120$	$^{249}\text{Bk}(^{51}\text{V}, 3n)$	330.00 d	234.9		0.001	[101]
	$^{249}\text{Bk}(^{51}\text{V}, 3n)$	330.00 d	230.0		0.0014	[104]
	$^{249}\text{Bk}(^{51}\text{V}, 3n)$	330.00 d	233.0		$0.0015^{+0.0024}_{-0.001}$	This work
$^{298}120$	$^{248}\text{Cm}(^{54}\text{Cr}, 4n)$	3.48×10^5 yr	248.9		0.0005	[36]
	$^{248}\text{Cm}(^{54}\text{Cr}, 4n)$	3.48×10^5 yr	250.1		0.005	[103]
	$^{248}\text{Cm}(^{54}\text{Cr}, 4n)$	3.48×10^5 yr	261.7		0.0003	[101]
	$^{248}\text{Cm}(^{54}\text{Cr}, 4n)$	3.48×10^5 yr	248.9		0.0005	[105]
	$^{248}\text{Cm}(^{54}\text{Cr}, 4n)$	3.48×10^5 yr	248.4		0.01	[106]
	$^{248}\text{Cm}(^{54}\text{Cr}, 4n)$	3.48×10^5 yr	250.0		0.003	[104]
	$^{248}\text{Cm}(^{54}\text{Cr}, 4n)$	3.48×10^5 yr	250.1		$0.0006^{+0.0013}_{-0.0004}$	This work
$^{299}120$	$^{248}\text{Cm}(^{54}\text{Cr}, 3n)$	3.48×10^5 yr	240.8		0.0007	[36]
	$^{248}\text{Cm}(^{54}\text{Cr}, 3n)$	3.48×10^5 yr	244.4		0.0008	[101]
	$^{248}\text{Cm}(^{54}\text{Cr}, 3n)$	3.48×10^5 yr	238.2		0.002	[103]
	$^{248}\text{Cm}(^{54}\text{Cr}, 3n)$	3.48×10^5 yr	240.7		0.0007	[105]
	$^{248}\text{Cm}(^{54}\text{Cr}, 3n)$	3.48×10^5 yr	240.0		0.0006	[104]
	$^{248}\text{Cm}(^{54}\text{Cr}, 3n)$	3.48×10^5 yr	242.1		$0.0004^{+0.0006}_{-0.0002}$	This work

$^{48}\text{Ca} + ^{242}\text{Pu} \rightarrow ^{290-xn}\text{Fl} + xn$, $^{48}\text{Ca} + ^{244}\text{Pu} \rightarrow ^{292-xn}\text{Fl} + xn$, $^{48}\text{Ca} + ^{243}\text{Am} \rightarrow ^{291-xn}\text{Mc} + xn$, $^{48}\text{Ca} + ^{245}\text{Cm} \rightarrow ^{293-xn}\text{Lv} + xn$, $^{48}\text{Ca} + ^{248}\text{Cm} \rightarrow ^{296-xn}\text{Lv} + xn$, $^{48}\text{Ca} + ^{249}\text{Bk} \rightarrow ^{297-xn}\text{Ts} + xn$ and $^{48}\text{Ca} + ^{249}\text{Cf} \rightarrow ^{297-xn}\text{Og} + xn$, as shown Fig. 1. The presence of theoretical computational uncertainties can be attributed to the subjective determination of the E_D range [98,99].

Figure 1 illustrates a reasonable agreement between the ER cross sections calculated by the DNS model and experimental data, with the deviations well within acceptable error margins. The DNS model predicts a maximal ER cross section of $1.41^{+1.98}_{-0.86}$ pb for the reaction $^{48}\text{Ca} + ^{238}\text{U} \rightarrow ^{286-xn}\text{Cn} + xn$ at the 3n-emission channel with $E_{\text{CN}}^* = 36.0$ MeV and $0.42^{+0.86}_{-0.30}$ pb for the reaction $^{48}\text{Ca} + ^{249}\text{Cf} \rightarrow ^{297-xn}\text{Og} + xn$ at the 3n-emission channel with $E_{\text{CN}}^* = 33.0$ MeV, which agrees well with the experimental value of $2.5^{+1.8}_{-1.1}$ pb with $E_{\text{CN}}^* =$ 33.0–37.0 MeV for the former reaction and $0.5^{+1.6}_{-0.3}$ pb with $E_{\text{CN}}^* = 32.1$–36.6 MeV for the latter at the same neutron-emission channel. Notably, the subjective selection range of E_D can result in an order of magnitude error range in the calculated ER cross sections. As the number of evaporated neutrons increases, the influence of E_D intensifies, resulting in an expanded error range. However, it is worth noting that the optimal incident energies are not sensitive to the E_D range. In Fig. 1, it also reveals that the Coulomb barrier heights in side-side collisions (V_B^{side}) are close to the optimal incident energies, which is consistent with both experiments and theoretical outcomes in Ref. [29,97]. These results provide strong support for the application of the DNS model in predicting the optimal projectile-target combinations and the corresponding incident energies for synthesizing unknown SHEs.
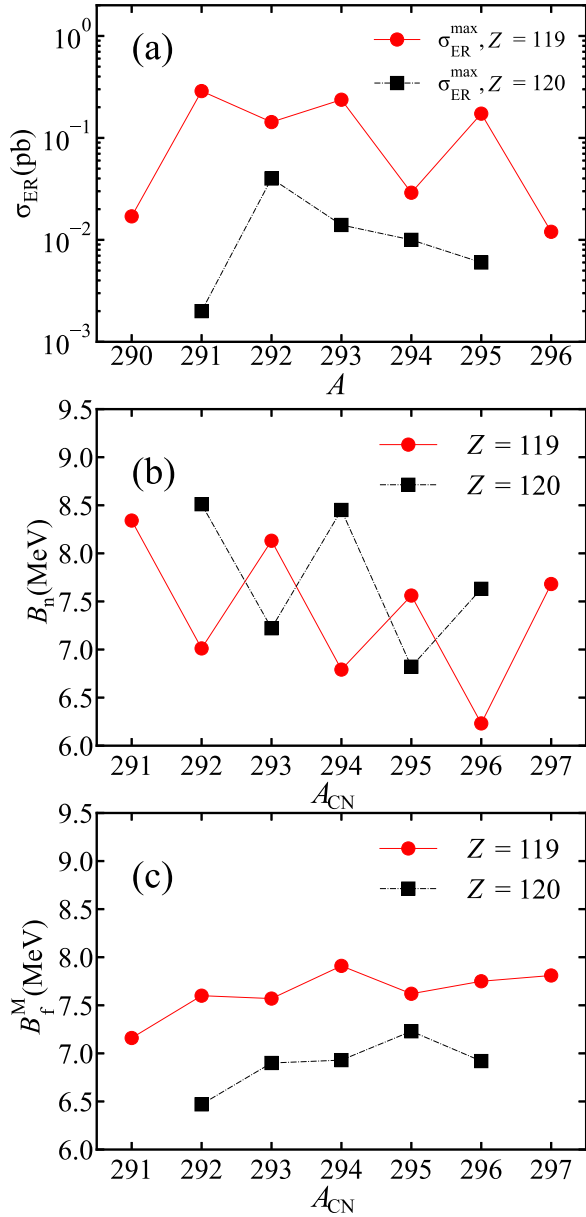
FIG. 2. (a) The predicted maximal ER cross sections for producing the isotopes of the SHE with $Z = 119$ (red solid line) and 120 (black dash-dot line). (b) The B_n of the compound nuclei which form the isotopes with $Z = 119$ (red solid lines) and 120 (black dash-dot lines). (c) The B_f^M of the compound nuclei which form the isotopes with $Z = 119$ (red solid lines) and 120 (black dash-dot lines).

FIG. 3. The calculated capture cross sections (a), fusion probabilities (b), and ER cross sections (c) of the reactions ^{45}Sc + ^{249}Cf (solid lines) and ^{50}V + ^{244}Cm (dash-dot lines). The ER cross sections in the 3n- and 4n-emission channels are denoted by the blue and red lines, respectively. The calculation uncertainties are given by the shaded areas.

III. RESULTS AND DISCUSSION

A. The analysis of maximal ER cross sections for synthesizing the SHEs with $Z = 119$ and 120

To select conducive projectile-target combinations for synthesizing the SHEs with $Z = 119$ and 120, a systematic evaluation of the combinations involving experimentally feasible actinide targets and stable projectiles is conducted within the DNS model. The maximal ER cross sections and the optimal incident energies of the feasible reaction systems
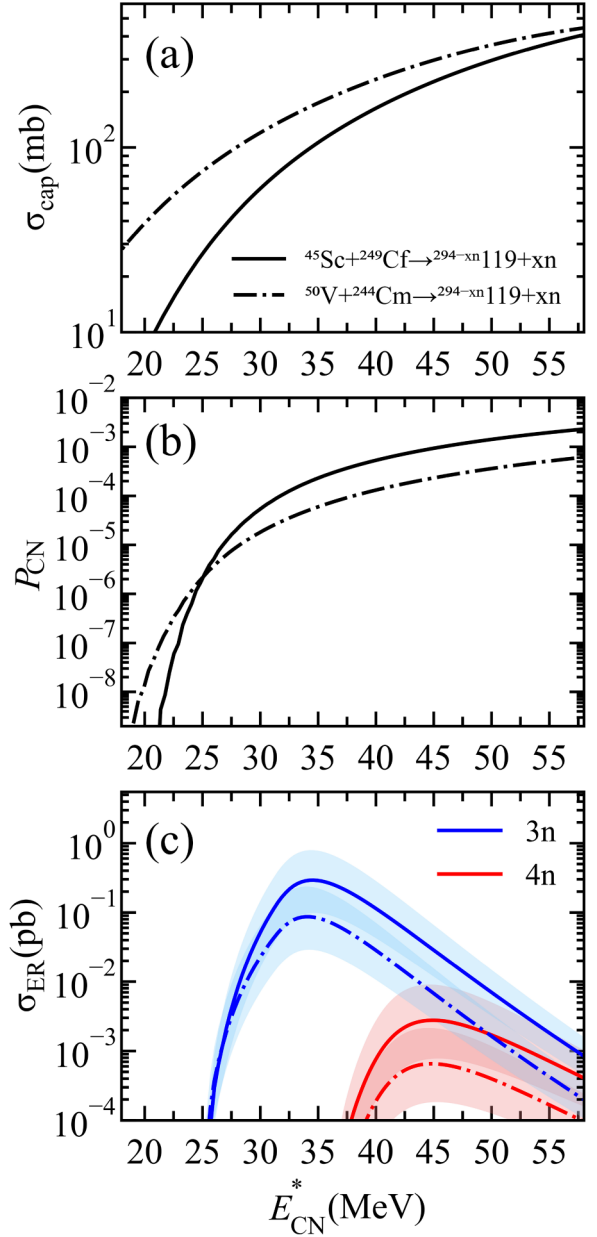
predicted by the DNS model and other theoretical models are presented in Table I. Notably, for the synthesis of a new element with $Z = 119$, the reaction ^{45}Sc + ^{249}Cf is predicted to be optimal by the DNS model, with a maximal ER cross section of 0.288 pb and optimal incident energy of 211.2 MeV. Besides, we predict V-induced reactions to be viable in the synthesis of the isotopes with $Z = 119$, such as the reaction ^{50}V + ^{246}Cm yielding a maximal ER cross section of 0.237 pb with a corresponding incident energy of 226.2 MeV.
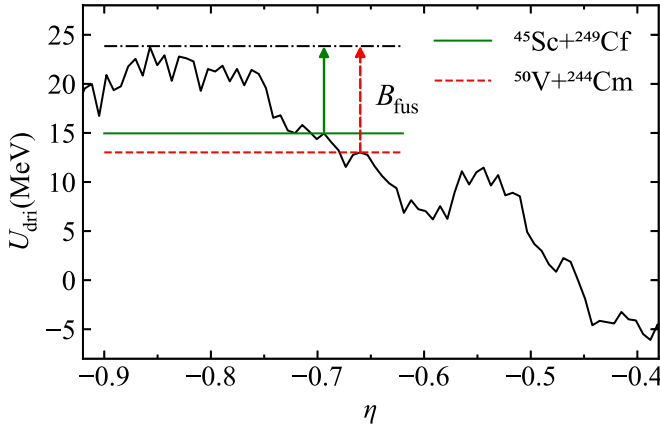
FIG. 4. The driving potential as a function of mass asymmetry. The B_{fus} values of the reactions $^{45}Sc + ^{249}Cf$ and $^{50}V + ^{244}Cm$ are represented by the green solid line arrow and red dashed line arrow, respectively.

In Table I, we also compare the optimal incident energies and maximal ER cross sections of this work with other theoretical models for producing new isotopes $^{294-296}119$ via the reactions $^{50}Ti + ^{249}Bk$, $^{51}V + ^{248}Cm$, and $^{54}Cr + ^{243}Am$. It is evident that the 4n-emission channel of the reaction $^{50}Ti + ^{249}Bk$ is advantageous in the synthesis of new element with $Z = 119$, where the predicted ER cross sections spans from 0.010 to 0.064 pb, aligning with the optimal incident energies in the range of 231.8 to 243.6 MeV.

Regarding the production of the SHE with $Z = 120$, the maximal ER cross sections and the optimal incident energies of some feasible reaction systems predicted by the DNS model and other theoretical approaches are presented in Table II. It indicates that the ER cross sections for producing isotopes with $Z = 120$ exhibit relatively lower values, and the DNS model predicts that the Ti-induced reactions are more promising, with the maximal ER cross section to be 0.040 pb achieved through the reaction $^{46}Ti + ^{249}Cf$ at an incident

energy of 221.8 MeV. Additionally, the maximal ER cross sections of the reactions $^{47,48}Ti + ^{249}Cf$ are also above 10 fb.

From Table II, the theoretical results of different models for the synthesis of new isotopes $^{295-299}120$ via the reactions $^{50}Ti + ^{249}Cf$, $^{51}V + ^{249}Bk$, and $^{54}Cr + ^{248}Cm$ are also compared. Most models predict that the 3n-emission channel of the reaction $^{50}Ti + ^{249}Cf$ is favorable for producing $Z = 120$, with the predicted ER cross sections ranging from 0.0023 to 0.042 pb and the optimal incident energies ranging from 227.4 to 236.6 MeV.

From Tables I and II, it is suggested that the calculated maximal ER cross sections of this work agree with other theoretical predictions within the error range. It is essential to note that the optimal incident energies of the same reaction system predicted by different theoretical models exhibit a discrepancy ranging from 0.2 to 13.6 MeV. The difference in the theoretical predictions arises from distinct interpretations of the physical processes underlying fusion-evaporation mechanisms. Besides, different mass tables provides distinct Physical quantities, including the Q, E_D, B_f^M, and B_n values, which impact the theoretical results.

In comparison to the synthesis of the SHE with $Z = 120$, the projectile-target combinations synthesizing the SHE with $Z = 119$ generally exhibit larger maximal ER cross sections. To further discuss this difference, we have plotted the maximal ER cross sections and B_n and B_f^M values for producing the new isotopes with $Z = 119$ and $Z = 120$ in Fig. 2.

From Fig. 2(a), it can be observed that the maximal ER cross sections for producing isotopes $^{291,293,295}119$ are enhanced. This enhancement can be attributed to the compound nuclei involved in the formation of these isotopes, which exhibit relatively lower B_n in Fig. 2(b). Consequently, these compound nuclei are more inclined to undergo deexcitation via neutron emission rather than fission. Moreover, Fig. 2(a) also reveals a suppression in the maximal ER cross sections for producing isotopes with $Z = 120$ comparing to those with $Z = 119$. This is mainly due to the reduced B_f^M values of the compound nuclei with $Z = 120$ in Fig. 2(c). As a
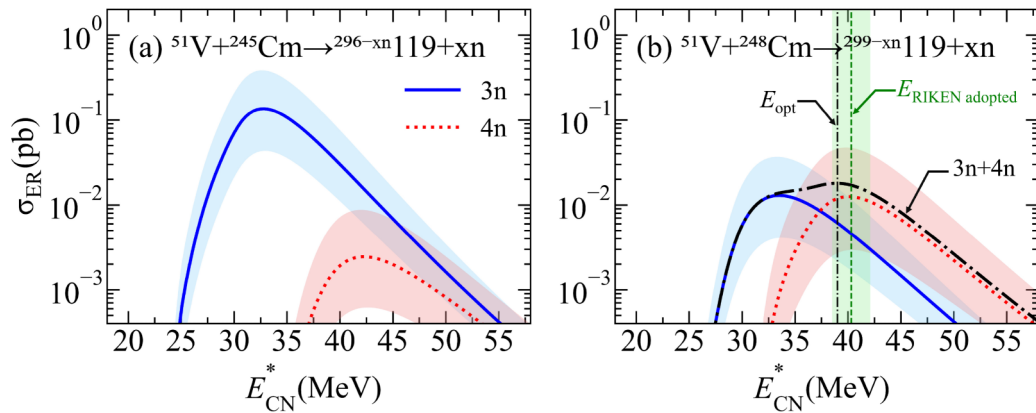

FIG. 5. The predicted ER cross sections of the reactions $^{51}V + ^{245}Cm$ (a) and $^{51}V + ^{248}Cm$ (b). The 3n- and 4n-emission channels are indicated by the blue solid and red dotted lines, respectively. The ER cross sections of the 3n + 4n channels in the reaction $^{51}V + ^{248}Cm$ are indicated by the black dash-dot line. The optimal reaction energy of the reaction $^{51}V + ^{248}Cm$ in the 3n + 4n channels from Ref. [29] and from this work are represented by the green dashed and black dash-dot lines, respectively. The calculation uncertainties are given by the shaded areas.
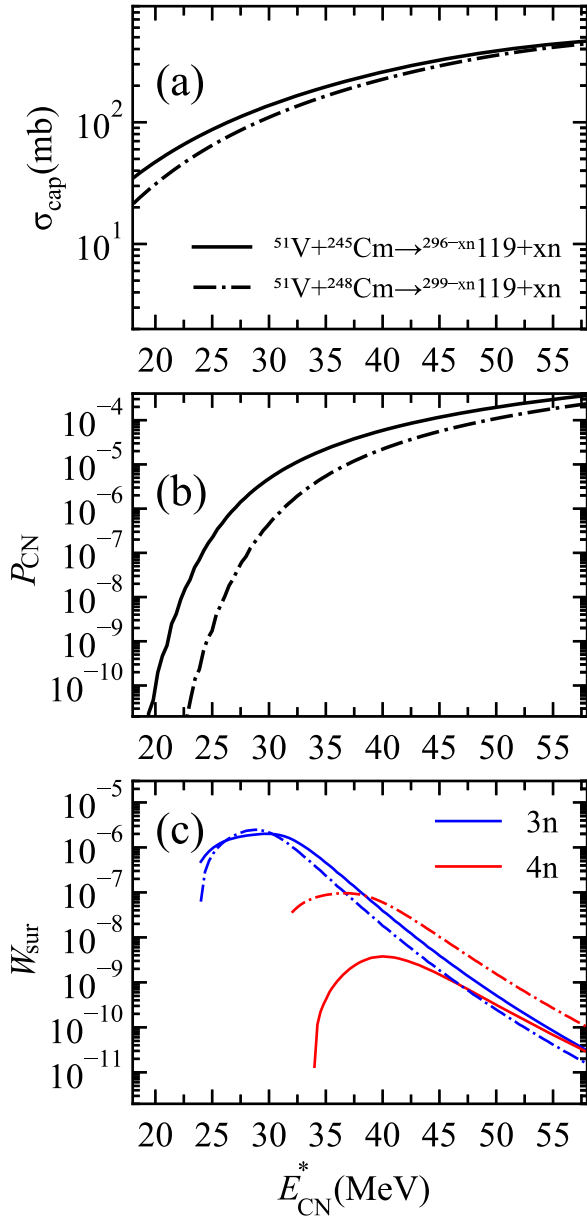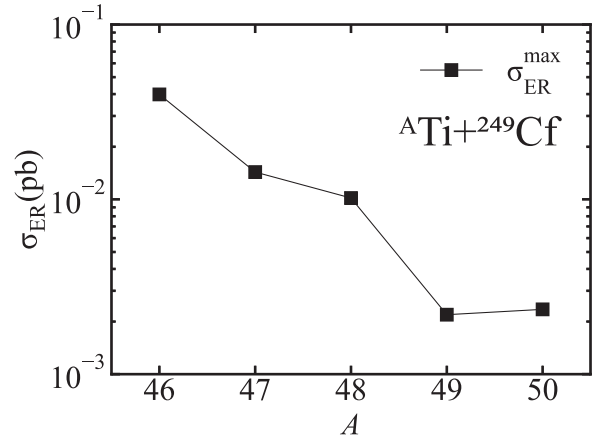
FIG. 7. The predicted maximal ER cross sections for producing the isotopes of the SHE with $Z = 120$ with ^{249}Cf target and $^{46-50}$Ti beams.

FIG. 6. The calculated capture cross sections (a), fusion probabilities (b), and survival probabilities (c) of the reactions ^{51}V + ^{245}Cm (solid lines) and ^{51}V + ^{248}Cm (dash-dot lines). The survival probabilities in the $3n$- and $4n$-emission channels are denoted by the blue and red lines, respectively.

consequence, the elevated probability of fission hinders the survival of compound nuclei. In light of these results, for forthcoming experiments aimed at synthesizing the new elements with $Z = 119$ and 120, we hope for a focus on the $3n$- and $4n$-emission channels of the compound nuclei with higher B_f^M and lower B_n values.

B. The entrance channel effect for the synthesis of the SHE with $Z = 119$

As previously discussed, for the synthesis of the SHE with $Z = 119$, the reaction ^{45}Sc + ^{249}Cf stands out with the largest

maximal ER cross section of 0.288 pb. Notably, this value exceeds that of the ^{50}V + ^{244}Cm reaction, even though both reactions form the same compound nucleus. To gain deeper insights into the effect of the entrance channel, the capture cross sections, the fusion probabilities, and the calculated ER cross sections of the reactions ^{45}Sc + ^{249}Cf and ^{50}V + ^{244}Cm are plotted in Fig. 3.

Owing to the increasing probability of overcoming the Coulomb barrier and the inner fusion barrier, both the capture cross sections and fusion probabilities elevate with rising E_{CN}^*. In Fig. 3(a), it is apparent that the capture cross section for ^{45}Sc + ^{249}Cf is relatively suppressed, which is attributed to the higher $V_B + Q$ value. However, this discrepancy decreases when E_{CN}^* exceeds $V_B + Q$, as the partial cross sections contribute at the larger angular momentum. Figure 3(b) reveals that the fusion probability of the reaction ^{50}V + ^{244}Cm is enhanced in the low-E_{CN}^* region owing to the much lower Q value. With relatively lower mass asymmetry, the incident point of the reaction ^{45}Sc + ^{249}Cf is closer to the B.G. point, resulting in B_{fus} of the reaction ^{45}Sc + ^{249}Cf (8.79 MeV) being lower than that of the reaction ^{50}V + ^{244}Cm (10.72 MeV), as shown in Fig. 4, and heightened likelihood of nucleon transfer process along the η degree. Therefore, the fusion probability of the reaction ^{45}Sc + ^{249}Cf surpasses that of the reaction ^{50}V + ^{244}Cm in the high-E_{CN}^* region, resulting in the enhancement of ER cross sections as plotted in Fig. 3(c).

Furthermore, for synthesizing the same isotopes ^{292}119 and ^{293}119 via the $3n$-emission channels, the ER cross sections using ^{50}V projectile are about two times lager than using the ^{51}V projectile. This difference can also be attributed to the enhanced fusion probability of the ^{50}V-induced reactions owing to the low mass asymmetry. It is evident that the reduced B_{fus} arising from the decreased mass asymmetry can highly enhance the fusion probability, and the reaction systems with lower mass asymmetry can therefore enhance the yield of desired isotopes.
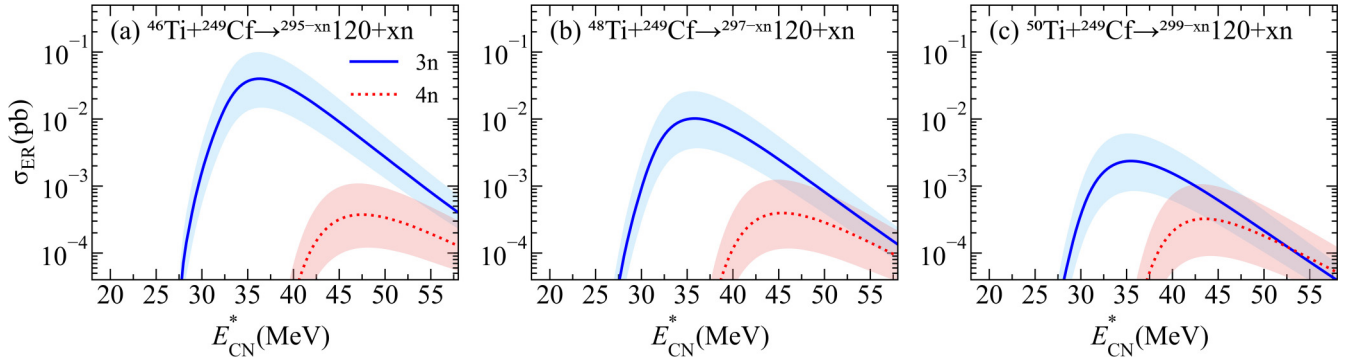
FIG. 8. The predicted ER cross sections of the reactions ^{46}Ti + ^{249}Cf (a), ^{48}Ti + ^{249}Cf (b), and ^{50}Ti + ^{249}Cf (c). The 3n- and 4n-emission channels are indicated by the solid and dotted lines, respectively. The calculation uncertainties are given by the shaded areas.

C. The isotopic dependence of targets for the synthesis of the SHE with $Z = 119$

As is evident in Table I, a variety of Cm targets can be practically used to synthesize the new isotopes $^{291-296}$119 with detectable maximal ER cross sections. Among the Cm-based fusion reactions, the reaction ^{50}V + ^{246}Cm is promising, with the highest maximal ER cross section of 0.237 pb in the 3n-emission channel. In Fig. 5, we present the predicted ER cross sections of ^{51}V + ^{245,248}Cm. Our results indicate that the maximal ER cross section of the reaction ^{51}V + ^{245}Cm in Fig. 5(a) is about one order of magnitude higher than that of the reaction ^{51}V + ^{248}Cm in Fig. 5(b). Remarkably, by investigating the V_{B}^{side} value extracted from the quasielastic barrier distribution measurement and the experimental data for the ER cross sections of 3n + 4n channels in the reaction ^{48}Ca + ^{248}Cm, a possible connection between the optimal incident energy and the V_{B}^{side} is found in Ref. [29], and the optimal reaction energy for producing the element with $Z = 119$ via the reaction ^{51}V + ^{248}Cm is estimated to be $234.8^{+1.8}_{-1.8}$ MeV with corresponding excitation energy of $40.3^{+1.8}_{-1.8}$ MeV near the 4n-emission channel. This result is consistent with our calculation of 234.0 MeV with an excitation energy of 39.0 MeV as shown in Fig. 5(b). As the fusion reaction embodies a complex interplay of the capture, fusion, and survival stages, to further investigate the isotopic dependence of Cm targets, the capture cross sections, fusion probabilities, and survival probabilities of the reactions ^{51}V + ^{245,248}Cm are discussed in Fig. 6.

In Fig. 6(a), the capture cross sections for both ^{51}V-induced reactions are quite similar. This similarity arises from the relatively close V_B and Q values. However, a contrast emerges in Fig. 6(b), where the fusion probability of the reaction ^{51}V + ^{245}Cm exceeds that of ^{51}V + ^{248}Cm by an order of magnitude. This can be attributed to the relatively lower B_{fus} of the reaction ^{51}V + ^{245}Cm (11.55 MeV), which is 2.53 MeV lower than that of the reaction ^{51}V + ^{248}Cm. As a result, the fusion probability of the reaction ^{51}V + ^{248}Cm is lower, especially in the low-E_{CN}^{*} region.

In Fig. 6(c), It can be observed that the survival probabilities in the 3n-emission channels for the two ^{51}V-induced reactions are relatively similar, which can be attributed to

the relatively small difference in B_n and B_f^{M} values of the corresponding compound nuclei. With the enhancement of the fusion probability, the maximal ER cross section of the reaction ^{51}V + ^{245}Cm appears in the 3n-emission channel, and is about an order of magnitude higher than that of the reaction ^{51}V + ^{248}Cm. Furthermore, Fig. 6(c) also reveals that the survival probability of the reaction ^{51}V + ^{248}Cm in the 4n-emission channel is higher. This can be ascribed to the much lower B_n value of the compound nucleus, leading to a higher probability of deexcitation via neutron emission. Additionally, the increasing E_{CN}^{*} also amplifies both the capture cross section and fusion probability. Consequently, the optimal incident energy is achieved at the 4n-emission channel for the reaction ^{51}V + ^{248}Cm.

D. The isotopic dependence of projectiles for the synthesis of the SHE with $Z = 120$

Among the limited projectile-target combinations for synthesizing the SHE with $Z = 120$ in Table II, the reaction ^{46}Ti + ^{249}Cf has the largest maximal ER cross section of 0.040 pb, at an incident energy of 221.8 MeV in the 3n-emission channel. Additionally, the maximal ER cross sections of the reactions ^{47,48}Ti + ^{249}Cf are also above the detection limit of 0.010 pb. These results suggest that the Ti-induced reactions with lower Coulomb repulsion are promising options for synthesizing the SHE with $Z = 120$. In Fig. 7, the calculated maximal ER cross sections of the reactions $^{46-50}$Ti + ^{249}Cf are plotted. It is evident that the maximal ER cross section has an obvious decreasing trend with increasing neutron richness of the Ti projectile.

To further discuss the isotopic dependence of the Ti projectiles on the maximal ER cross sections, Fig. 8 displays the calculated ER cross sections of the reactions ^{46,48,50}Ti + ^{249}Cf. One can observe that the optimal incident energies of these reactions appear in the 3n-emission channels. To further discuss the isotopic dependence of projectiles, the capture cross sections, the fusion probabilities and the survival probabilities of the reactions ^{46,48,50}Ti + ^{249}Cf are plotted in Fig. 9.

As the neutron number of the projectile increases, the capture cross sections have a rising trend as plotted in Fig. 9(a)
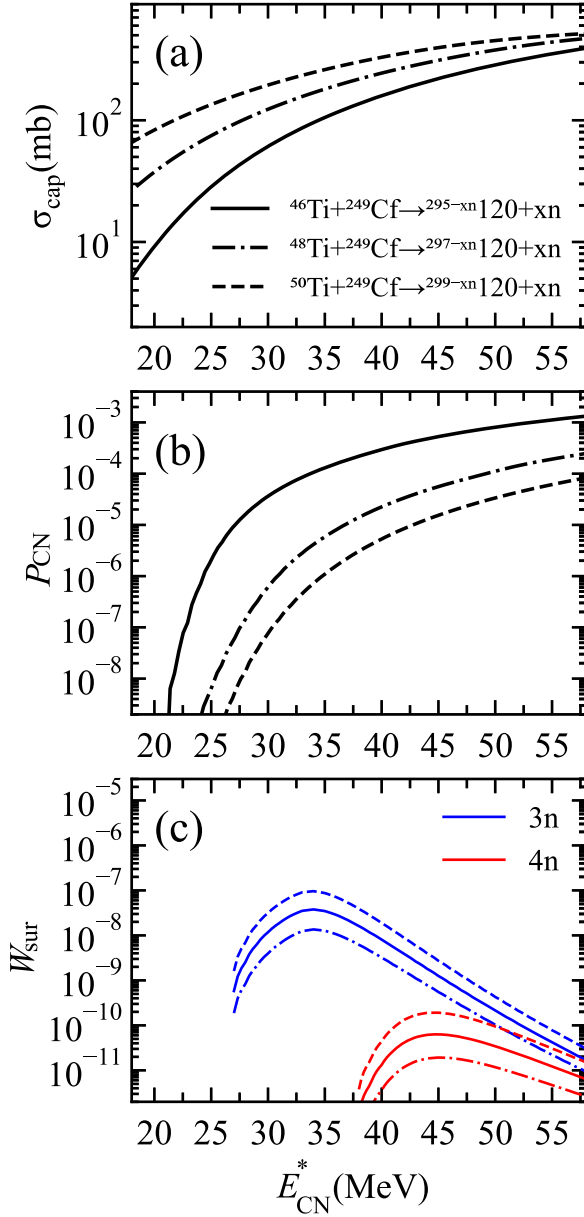
FIG. 9. The calculated capture cross sections (a), fusion probabilities (b), and survival probabilities (c) of the reactions ^{46}Ti + ^{249}Cf (solid lines), ^{48}Ti + ^{249}Cf (dash-dot lines) and ^{50}Ti + ^{249}Cf (dashed lines). The survival probabilities in the 3n- and 4n-emission channels are denoted by the blue and red lines, respectively.

owing to the the diminishing $V_B + Q$ values [55]. In the fusion stage, the heavier projectile increases the mass asymmetry,

resulting in the increased B_{fus}, and the fusion probability is suppressed by several orders of magnitude, as shown in Fig. 9(b). In Fig. 9(c), one can observe that the survival probabilities rise with heavier Ti beams, due to the enhanced stability of the compound nucleus when the neutron number approaches the predicted closed neutron shell with $N = 184$. Despite the suppression in the capture and survival stages, The maximal ER cross section of the reaction ^{46}Ti + ^{249}Cf remains relatively large because of the strongly enhanced fusion probability. Given the enhancement in the fusion stage resulting, the reaction ^{46}Ti + ^{249}Cf can be considered for future experiments to synthesize the element with $Z = 120$.

IV. CONCLUSION

In this paper, the calculated ER cross sections within the DNS model are examined with the experimental data of the reactions ^{48}Ca + ^{238}U, ^{242,244}Pu, ^{243}Am, ^{245,248}Cm, ^{249}Bk, and ^{249}Cf. The calculated results are found to be consistent with the experimental data within the error ranges. This work attempts to synthesize the SHEs with $Z = 119$ and 120 using stable projectiles with $Z > 20$ and experimentally feasible actinide targets, and the analysis of projectile-target combinations reveals that the element with $Z = 119$ is expected to be produced via the reactions ^{45}Sc + ^{249}Cf and ^{50}V + ^{246}Cm, achieving maximal ER cross sections of 0.288 and 0.237 pb with corresponding incident energies of 211.2 and 226.2 MeV. The fusion reaction ^{46}Ti + ^{249}Cf is a promising option to synthesize the new element with $Z = 120$, reaching a maximal ER cross section of 0.040 pb at the incident energy of 221.8 MeV. The isotopes with $Z = 119$ and 120 are suggested to be synthesized via the 3n- and 4n-emission channels of the compound nuclei with low B_n and high B_f^M values. For the synthesis of the SHE with $Z = 119$, the entrance channel effect and the isotopic dependence of the Cm targets are discussed. Our findings reveal that the reaction systems with low mass asymmetry and the neutron-deficient Cm targets can be employed to enhance the maximal ER cross sections. Furthermore, the isotopic dependence of the Ti beams for the synthesis of the element with $Z = 120$ is also investigated, suggesting that the raised fusion probability from the employment of the neutron-deficient ^{46}Ti beam can enhance the maximal ER cross section.

[1] M. Thoennessen, *The Discovery of Isotopes: A Complete Compilation* (Springer International Publishing, New York, 2016).

[2] P. Möller, A. J. Sierk, T. Ichikawa, and H. Sagawa, At. Data Nucl. Data Tables **109-110**, 1 (2016).

[3] S. Ćwiok, P. H. Heenen, and W. Nazarewicz, Nature (London) **433**, 705 (2005).

[4] A. T. Kruppa, M. Bender, W. Nazarewicz, P. G. Reinhard, T. Vertse, and S. Ćwiok, Phys. Rev. C **61**, 034313 (2000).

[5] D. Ackermann and C. Theisen, Phys. Scr. **92**, 083002 (2017).

[6] K. Morita, K. Morimoto, D. Kaji, T. Akiyama, S. Goto, H. Haba, E. Ideguchi, R. Kanungo, K. Katori, H. Koura, H. Kudo, T. Ohnishi, A. Ozawa, T. Suda, K. Sueki, H. S. Xu, T. Yamaguchi, A. Yoneda, A. Yoshida, and Y. L. Zhao, J. Phys. Soc. Jpn. **73**, 2593 (2004).

[7] S. Hofmann and G. Münzenberg, Rev. Mod. Phys. **72**, 733 (2000).

[8] Y. T. Oganessian and V. K. Utyonkov, Rep. Prog. Phys. **78**, 036301 (2015).

[9] Y. T. Oganessian, V. K. Utyonkov, Y. V. Lobanov, F. S. Abdullin, A. N. Polyakov, R. N. Sagaidak, I. V. Shirokovsky, Y. S. Tsyganov, A. A. Voinov, G. G. Gulbekian, S. L. Bogomolov, B. N. Gikal, A. N. Mezentsev, S. Iliev, V. G. Subbotin, A. M. Sukhov, K. Subotic, V. I. Zagrebaev, G. K. Vostokin, M. G. Itkis *et al.*, Phys. Rev. C **74**, 044602 (2006).

[10] Y. T. Oganessian, A. V. Yeremin, A. G. Popeko, S. L. Bogomolov, G. V. Buklanov, M. L. Chelnokov, V. I. Chepigin, B. N. Gikal, V. A. Gorshkov, G. G. Gulbekian *et al.*, Nature (London) **400**, 242 (1999).

[11] Y. T. Oganessian, F. S. Abdullin, S. N. Dmitriev, J. M. Gostic, J. H. Hamilton, R. A. Henderson, M. G. Itkis, K. J. Moody, A. N. Polyakov, A. V. Ramayya, J. B. Roberto, K. P. Rykaczewski, R. N. Sagaidak, D. A. Shaughnessy, I. V. Shirokovsky, M. A. Stoyer, N. J. Stoyer, V. G. Subbotin, A. M. Sukhov, Y. S. Tsyganov, V. K. Utyonkov, A. A. Voinov, and G. K. Vostokin, Phys. Rev. C **87**, 014302 (2013).

[12] Y. T. Oganessian, V. K. Utyonkov, Y. V. Lobanov, F. S. Abdullin, A. N. Polyakov, I. V. Shirokovsky, Y. S. Tsyganov, G. G. Gulbekian, S. L. Bogomolov, B. N. Gikal, A. N. Mezentsev, S. Iliev, V. G. Subbotin, A. M. Sukhov, O. V. Ivanov, G. V. Buklanov, K. Subotic, M. G. Itkis, K. J. Moody, J. F. Wild, N. J. Stoyer, M. A. Stoyer, R. W. Lougheed, C. A. Laue, Y. A. Karelin, and A. N. Tatarinov, Phys. Rev. C **63**, 011301(R) (2000).

[13] Y. T. Oganessian, F. S. Abdullin, P. D. Bailey, D. E. Benker, M. E. Bennett, S. N. Dmitriev, J. G. Ezold, J. H. Hamilton, R. A. Henderson, M. G. Itkis, Y. V. Lobanov, A. N. Mezentsev, K. J. Moody, S. L. Nelson, A. N. Polyakov, C. E. Porter, A. V. Ramayya, F. D. Riley, J. B. Roberto, M. A. Ryabinin *et al.*, Phys. Rev. Lett. **104**, 142502 (2010).

[14] H. Sakai, H. Haba, K. Morimoto, and N. Sakamoto, Eur. Phys. J. A **58**, 238 (2022).

[15] G. G. Gulbekian, S. N. Dmitriev, M. G. Itkis, Y. T. Oganessyan, B. N. Gikal, I. V. Kalagin, V. A. Semin, S. L. Bogomolov, V. A. Buzmakov, I. A. Ivanenko, N. Y. Kazarinov, N. F. Osipov, S. V. Pashenko, V. A. Sokolov, N. N. Pchelkin, S. V. Prokhorov, M. V. Khabarov, and G. K. B, Phys. Part. Nucl. Lett. **16**, 866 (2019).

[16] J. H. Hamilton, S. Hofmann, and Y. T. Oganessian, Ann. Rev. Nucl. Part. Sci. **63**, 383 (2013).

[17] L. J. Mao, J. C. Yang, J. W. Xia, Y. J. Yuan, P. Yuan, W. M. Qiao, D. Q. Gao, G. Q. Xiao, H. W. Zhao, H. S. Xu, M. T. Song, X. D. Yang, X. H. Cai, L. Z. Ma, X. T. Yang, K. T. Man, Y. He, Z. Z. Zhou, J. H. Zhang, Z. Xu *et al.*, J. Instrum. **15**, T12015 (2020).

[18] W. Barth, W. Bayer, L. Dahl, L. Groening, S. Richter, and S. Yaramyshev, Nucl. Instrum. Methods. Phys. Res. A **577**, 211 (2007).

[19] https://people.nscl.msu.edu/~thoennes/isotopes/index.html.

[20] Y. T. Oganessian and V. K. Utyonkov, Nucl. Phys. A **944**, 62 (2015).

[21] M. Thoennessen, At. Data Nucl. Data Tables **99**, 312 (2013).

[22] Z. Y. Zhang, Z. G. Gan, L. Ma, M. H. Huang, T. H. Huang, X. L. Wu, G. B. Jia, G. S. Li, L. Yu, and Z. Z. Ren, Chin. Phys. Lett **29**, 012502 (2012).

[23] Y. T. Oganessian, V. K. Utyonkov, N. D. Kovrizhnykh, F. S. Abdullin, S. N. Dmitriev, A. A. Dzhioev, D. Ibadullayev, M. G. Itkis, A. V. Karpov, D. A. Kuznetsov, O. V. Petrushkin, A. V. Podshibiakin, A. N. Polyakov, A. G. Popeko, I. S. Rogov, R. N. Sagaidak, L. Schlattauer, V. D. Shubin, M. V. Shumeiko, D. I. Solovyev *et al.*, Phys. Rev. C **106**, 064306 (2022).

[24] S. Hofmann, Radiochim. Acta **99**, 405 (2011).

[25] Y. T. Oganessian, V. K. Utyonkov, Y. V. Lobanov, F. S. Abdullin, A. N. Polyakov, R. N. Sagaidak, I. V. Shirokovsky, Y. S. Tsyganov, A. A. Voinov, A. N. Mezentsev, V. G. Subbotin, A. M. Sukhov, K. Subotic, V. I. Zagrebaev, S. N. Dmitriev, R. A. Henderson, K. J. Moody, J. M. Kenneally, J. H. Landrum, D. A. Shaughnessy, M. A. Stoyer, N. J. Stoyer, and P. A. Wilk, Phys. Rev. C **79**, 024603 (2009).

[26] S. Hofmann, S. Heinz, R. Mann, J. Maurer, G. Münzenberg, S. Antalic, W. Barth, H. Burkhard, L. Dahl *et al.*, Eur. Phys. J. A **52**, 116 (2016).

[27] F. P. Heßberger and D. Ackermann, Eur. Phys. J. A **53**, 123 (2017).

[28] J. Khuyagbaatar, A. Yakushev, C. E. Düllmann, D. Ackermann, L. L. Andersson, M. Asai, M. Block, R. A. Boll, H. Brand, D. M. Cox, M. Dasgupta, X. Derkx, A. Di Nitto, K. Eberhardt, J. Even, M. Evers, C. Fahlander, U. Forsberg, J. M. Gates, N. Gharibyan *et al.*, Phys. Rev. C **102**, 064602 (2020).

[29] M. Tanaka, P. Brionnet, M. Du, J. Ezold, K. Felker, B. J. Gall, S. Go, R. K. Grzywacz, H. Haba, K. Hagino, S. Hogle, S. Ishizawa, D. Kaji, S. Kimura, T. T. King, Y. Komori, R. K. Lemon, M. G. Leonard, K. Morimoto, K. Morita *et al.*, J. Phys. Soc. Jpn. **91**, 084201 (2022).

[30] Z. S. Ge, G. Zhang, S. H. Cheng, Y. S. Tsyganov, and F. S. Zhang, Chin. Phys. C **44**, 104102 (2020).

[31] T. K. Dong, Z. Z. Ren, and C. Xu, Chin. Phys. C **33**, 5 (2009).

[32] Y. T. Oganessian, J. Phys.: Conf. Ser. **337**, 012005 (2012).

[33] Y. H. Zhang, G. Zhang, J. J. Li, Z. Liu, A. V. Yeremin, and F. S. Zhang, Phys. Rev. C **106**, 014625 (2022).

[34] N. Wang, Z. X. Li, and X. Z. Wu, Phys. Rev. C **65**, 064608 (2002).

[35] Z. H. Liu and J. D. Bao, Phys. Rev. C **80**, 054608 (2009).

[36] K. Siwek-Wilczyńska, T. Cap, M. Kowal, A. Sobiczewski, and J. Wilczyński, Phys. Rev. C **86**, 014611 (2012).

[37] X. X. Sun and L. Guo, Phys. Rev. C **107**, 064609 (2023).

[38] S. Chopra, M. K. Sharma, P. O. Hess, and J. Bedi, Phys. Rev. C **105**, 014610 (2022).

[39] P. Magierski, K. Sekizawa, and G. Wlazłowski, Phys. Rev. Lett. **119**, 042501 (2017).

[40] A. S. Umar, V. E. Oberacker, J. A. Maruhn, and P. G. Reinhard, Phys. Rev. C **81**, 064607 (2010).

[41] K. Sekizawa and K. Hagino, Phys. Rev. C **99**, 051602(R) (2019).

[42] L. Liu, C. W. Shen, Q. F. Li, Y. Tu, X. B. Wang, and Y. J. Wang, Eur. Phys. J. A **52**, 35 (2016).

[43] C. W. Shen, Y. Abe, D. Boilley, G. Kosenko, and E. G. Zhao, Int. J. Mod. Phys. E **17**, 66 (2008).

[44] D. Boilley, Y. Abe, B. Cauchois, and C. W. Shen, J. Phys. G: Nucl. Part. Phys. **46**, 115102 (2019).

[45] V. L. Litnevsky, G. I. Kosenko, and F. A. Ivanyuk, Phys. Rev. C **93**, 064606 (2016).

[46] V. L. Litnevsky, V. V. Pashkevich, G. I. Kosenko, and F. A. Ivanyuk, Phys. Rev. C **89**, 034626 (2014).

[47] S. Amano, Y. Aritomo, and M. Ohta, Phys. Rev. C **108**, 014612 (2023).

[48] N. Wang, E. G. Zhao, W. Scheid, and S. G. Zhou, Phys. Rev. C **85**, 041601(R) (2012).

[49] G. G. Adamian, N. Antonenko, W. Scheid, and V. Volkov, Nucl. Phys. A **633**, 409 (1998).

[50] J. Hong, G. G. Adamian, and N. Antonenko, Phys. Lett. B **764**, 42 (2017).

[51] X. J. Bao, Y. Gao, J. Q. Li, and H. F. Zhang, Phys. Rev. C **92**, 034612 (2015).

[52] X. J. Bao, Y. Gao, J. Q. Li, and H. F. Zhang, Phys. Rev. C **91**, 011603(R) (2015).

[53] Z. Q. Feng, G. M. Jin, F. Fu, and J. Q. Li, Nucl. Phys. A **771**, 50 (2006).

[54] L. Zhu, Z. Q. Feng, C. Li, and F. S. Zhang, Phys. Rev. C **90**, 014612 (2014).

[55] L. Zhu, J. Su, and F. S. Zhang, Phys. Rev. C **93**, 064610 (2016).

[56] J. X. Li and H. F. Zhang, Phys. Rev. C **106**, 034613 (2022).

[57] F. Li, L. Zhu, Z. H. Wu, X. B. Yu, J. Su, and C. C. Guo, Phys. Rev. C **98**, 014618 (2018).

[58] S. H. Zhu and X. J. Bao, Phys. Rev. C **108**, 014604 (2023).

[59] J. X. Li and H. F. Zhang, Phys. Rev. C **108**, 044604 (2023).

[60] V. I. Zagrebaev, Phys. Rev. C **64**, 034606 (2001).

[61] A. S. Zubov, G. G. Adamian, N. V. Antonenko, S. P. Ivanova, and W. Scheid, Phys. Rev. C **65**, 024308 (2002).

[62] Z. Ahmed, Phys. Lett. A **157**, 1 (1991).

[63] V. Y. Denisov, Phys. Rev. C **107**, 054618 (2023).

[64] S. Rana, R. Kumar, S. Patra, and M. Bhuyan, Eur. Phys. J. A **58**, 241 (2022).

[65] W. D. Myers and W. J. Swiatecki, Nucl. Phys. **81**, 1 (1966).

[66] C. Y. Wong, Phys. Rev. Lett. **31**, 766 (1973).

[67] I. I. Gontchar, D. J. Hinde, M. Dasgupta, and J. O. Newton, Phys. Rev. C **69**, 024610 (2004).

[68] B. Wang, K. Wen, W. J. Zhao, E. G. Zhao, and S. G. Zhou, At. Data Nucl. Data Tables **114**, 281 (2017).

[69] N. Wang, L. Dou, E. G. Zhao, and W. Scheid, Chin. Phys. Lett. **27**, 062502 (2010).

[70] S. Ayik, B. Schürmann, and W. Nörenberg, Z. Phys. A **277**, 299 (1976).

[71] P. Grangé, L. Jun-Qing, and H. A. Weidenmüller, Phys. Rev. C **27**, 2063 (1983).

[72] G. G. Adamian, N. V. Antonenko, and W. Scheid, Phys. Rev. C **68**, 034601 (2003).

[73] K. H. Schmidt and W. Morawek, Rep. Prog. Phys. **54**, 949 (1991).

[74] X. J. Bao, S. Q. Guo, H. F. Zhang, and J. Q. Li, J. Phys. G: Nucl. Part. Phys. **43**, 125105 (2016).

[75] J. Q. Li and G. Wolschin, Phys. Rev. C **27**, 590 (1983).

[76] J. D. Jackson, Can. J. Phys. **34**, 767 (1956).

[77] V. Weisskopf, Phys. Rev. **52**, 295 (1937).

[78] A. V. Ignatyuk, K. K. Istekov, and G. N. Smirenkin, Sov. J. Nucl. Phys. **29**, 875 (1979).

[79] M. Blann, Phys. Rev. C **21**, 1770 (1980).

[80] G. G. Adamian, N. V. Antonenko, S. P. Ivanova, and W. Scheid, Phys. Rev. C **62**, 064303 (2000).

[81] A. S. Zubov, G. G. Adamian, N. V. Antonenko, S. P. Ivanova, and W. Scheid, Eur. Phys. J. A **23**, 249 (2005).

[82] L. Zhu, J. Phys. G: Nucl. Part. Phys. **47**, 065107 (2020).

[83] V. Y. Denisov and I. Y. Sedykh, Phys. Rev. C **98**, 024601 (2018).

[84] W. F. Li, Z. Z. Wang, H. S. Xu, Y. Ma, H. F. Zhang, W. Zuo, J. Q. Li, N. Wang, E. G. Zhao, and W. Scheid, Chin. Phys. Lett. **21**, 636 (2004).

[85] C. J. Xia, B. X. Sun, E. G. Zhao, and S. G. Zhou, Sci. China-Phys. Mech. Astron. **54**, 109 (2011).

[86] Y. T. Oganessian, V. K. Utyonkov, Y. V. Lobanov, F. S. Abdullin, A. N. Polyakov, I. V. Shirokovsky, Y. S. Tsyganov, G. G. Gulbekian, S. L. Bogomolov, B. N. Gikal, A. N. Mezentsev, S. Iliev, V. G. Subbotin, A. M. Sukhov, A. A. Voinov, G. V. Buklanov, K. Subotic, V. I. Zagrebaev, M. G. Itkis, J. B. Patin *et al.*, Phys. Rev. C **70**, 064609 (2004).

[87] Y. T. Oganessian, V. K. Utyonkov, N. D. Kovrizhnykh, F. S. Abdullin, S. N. Dmitriev, D. Ibadullayev, M. G. Itkis, D. A. Kuznetsov, O. V. Petrushkin, A. V. Podshibiakin, A. N. Polyakov, A. G. Popeko, R. N. Sagaidak, L. Schlattauer, I. V. Shirokovski, V. D. Shubin, M. V. Shumeiko, D. I. Solovyev, Y. S. Tsyganov, A. A. Voinov *et al.*, Phys. Rev. C **106**, L031301 (2022).

[88] Y. T. Oganessian, V. K. Utyonkov, D. Ibadullayev, F. S. Abdullin, S. N. Dmitriev, M. G. Itkis, A. V. Karpov, N. D. Kovrizhnykh, D. A. Kuznetsov, O. V. Petrushkin, A. V. Podshibiakin, A. N. Polyakov, A. G. Popeko, R. N. Sagaidak, L. Schlattauer, V. D. Shubin, M. V. Shumeiko, D. I. Solovyev, Y. S. Tsyganov, A. A. Voinov *et al.*, Phys. Rev. C **106**, 024612 (2022).

[89] Y. T. Oganessian, V. K. Utyonkov, Y. V. Lobanov, F. S. Abdullin, A. N. Polyakov, I. V. Shirokovsky, Y. S. Tsyganov, G. G. Gulbekian, S. L. Bogomolov, B. N. Gikal, A. N. Mezentsev, S. Iliev, V. G. Subbotin, A. M. Sukhov, A. A. Voinov, G. V. Buklanov, K. Subotic, V. I. Zagrebaev, M. G. Itkis, J. B. Patin *et al.*, Phys. Rev. C **69**, 054607 (2004).

[90] Y. T. Oganessian, V. K. Utyonkov, Y. V. Lobanov, F. S. Abdullin, A. N. Polyakov, I. V. Shirokovsky, Y. S. Tsyganov, G. G. Gulbekian, S. L. Bogomolov, A. N. Mezentsev, S. Iliev, V. G. Subbotin, A. M. Sukhov, A. A. Voinov, G. V. Buklanov, K. Subotic, V. I. Zagrebaev, M. G. Itkis, J. B. Patin, K. J. Moody *et al.*, Phys. Rev. C **69**, 021601(R) (2004).

[91] Y. T. Oganessian, F. S. Abdullin, C. Alexander, J. Binder, R. A. Boll, S. N. Dmitriev, J. Ezold, K. Felker, J. M. Gostic, R. K. Grzywacz, J. H. Hamilton, R. A. Henderson, M. G. Itkis, K. Miernik, D. Miller, K. J. Moody, A. N. Polyakov, A. V. Ramayya, J. B. Roberto, M. A. Ryabinin, K. P. Rykaczewski *et al.*, Phys. Rev. C **87**, 054621 (2013).

[92] Y. T. Oganessian, F. S. Abdullin, C. Alexander, J. Binder, R. A. Boll, S. N. Dmitriev, J. Ezold, K. Felker, J. M. Gostic, R. K. Grzywacz, J. H. Hamilton, R. A. Henderson, M. G. Itkis, K. Miernik, D. Miller, K. J. Moody, A. N. Polyakov, A. V. Ramayya, J. B. Roberto, M. A. Ryabinin *et al.*, Phys. Rev. Lett. **109**, 162501 (2012).

[93] A. A. Voinov, Y. T. Oganessian, F. S. Abdullin, N. T. Brewer, S. N. Dmitriev, R. K. Grzywacz, J. H. Hamilton, M. G. Itkis, K. Miernik, A. N. Polyakov *et al.*, J. Phys. Conf. **966**, 012057 (2018).

[94] L. Stavsetra, K. E. Gregorich, J. Dvorak, P. A. Ellison, I. Dragojević, M. A. Garcia, and H. Nitsche, Phys. Rev. Lett. **103**, 132502 (2009).

[95] P. A. Ellison, K. E. Gregorich, J. S. Berryman, D. L. Bleuel, R. M. Clark, I. Dragojević, J. Dvorak, P. Fallon, C. Fineman-

Sotomayor, J. M. Gates, O. R. Gothe, I. Y. Lee, W. D. Loveland, J. P. McLaughlin, S. Paschalis, M. Petri, J. Qian, L. Stavsetra, M. Wiedeking, and H. Nitsche, Phys. Rev. Lett. **105**, 182701 (2010).

[96] J. M. Gates, C. E. Düllmann, M. Schädel, A. Yakushev, A. Türler, K. Eberhardt, J. V. Kratz, D. Ackermann, L. L. Andersson, M. Block, W. Brüchle, J. Dvorak, H. G. Essel, P. A. Ellison, J. Even, U. Forsberg, J. Gellanki, A. Gorshkov, R. Graeger, K. E. Gregorich *et al.*, Phys. Rev. C **83**, 054618 (2011).

[97] L. Zhu, Phys. Rev. Res. **5**, L022030 (2023).

[98] H. L. Lü, D. Boilley, Y. Abe, and C. W. Shen, Phys. Rev. C **94**, 034616 (2016).

[99] J. A. Sheikh, W. Nazarewicz, and J. C. Pei, Phys. Rev. C **80**, 011302(R) (2009).

[100] http://nrv.jinr.ru/nrv/webnrv/map/ and https://people.nscl.msu.edu/thoennes/isotopes and https://www.nndc.bnl.gov/nudat3/.

[101] X. J. Lv, Z. Y. Yue, W. J. Zhao, and B. Wang, Phys. Rev. C **103**, 064616 (2021).

[102] V. Zagrebaev and W. Greiner, Phys. Rev. C **78**, 034610 (2008).

[103] N. Wang, J. Tian, and W. Scheid, Phys. Rev. C **84**, 061601(R) (2011).

[104] L. Zhu, W. J. Xie, and F. S. Zhang, Phys. Rev. C **89**, 024615 (2014).

[105] K. Siwek-Wilczyńska, T. Cap, and M. Kowal, Phys. Rev. C **99**, 054603 (2019).

[106] A. N. Kuzmina, G. G. Adamian, and N. V. Antonenko, Eur. Phys. J. A **47**, 145 (2011).